Chirped-pulse millimeter-wave spectroscopy for dynamics and kinetics studies of pyrolysis reactions

Massachusetts Institute of Technology

Chirped-pulse millimeter-wave spectroscopy for dynamics and kinetics studies of pyrolysis reactions

Kirill Prozument [1), 2)], G. Barratt Park [1)], Rachel G. Shaver [1)],

AnGayle K. Vasiliou [3)], James M. Oldham [2)], Donald E. David [4)],

John S. Muenter [5)], John F. Stanton [6)], Arthur G. Suits [2)],

G. Barney Ellison [4)], and Robert W. Field [1)]

[1)] Department of Chemistry, Massachusetts Institute of Technology, 77 Massachusetts Ave, Cambridge, MA 02139

[2)] Department of Chemistry, Wayne State University, 5101 Cass Ave, Detroit, MI 48202

[3)] Department of Chemistry and Biochemistry, Middlebury College, 276 Bicentennial Way, Middlebury, VT 05753

[4)] Department of Chemistry and Biochemistry, University of Colorado at Boulder, Cristol Chemistry 58, Boulder, CO 80309

[5)] Department of Chemistry, University of Rochester, 120 Trustee Road, Rochester, NY 14627

[6)] Department of Chemistry, The University of Texas at Austin, 1 University Station A5300, Austin, TX 78712-0165

28 March 2014

Abstract

A Chirped-Pulse millimeter-Wave (CPmmW) spectrometer is applied to the study of chemical reaction products that result from pyrolysis in a Chen nozzle heated to $1000 - 1800$ K. Millimeter-wave rotational spectroscopy unambiguously determines, for each polar reaction product, the species, the conformers, relative concentrations, conversion percentage from precursor to each product, and, in some cases, vibrational state population distributions. A chirped-pulse spectrometer can, within the frequency range of a single chirp, sample spectral regions of up to ~10 GHz and simultaneously detect many reaction products. Here we introduce a modification to the CPmmW technique in which multiple chirps *of different spectral content* are applied to a molecular beam pulse that contains the pyrolysis reaction products. This technique allows for controlled allocation of its sensitivity to specific molecular transitions and effectively doubles the bandwidth of the spectrometer. As an example, the pyrolysis reaction of ethyl nitrite, CH_3CH_2ONO, is studied at different temperatures of the Chen reactor, and CH_3CHO, H_2CO, and HNO products are simultaneously observed, exploiting the multi-chirp CPmmW technique. Rotational and vibrational temperatures of some product molecules are determined. Subsequent to supersonic expansion from the heated nozzle, acetaldehyde molecules display a rotational temperature of 4 ± 1 K. Vibrational temperatures are found to be controlled by the collisional cooling in the expansion, and to be both species- and vibrational mode-dependent. Rotational transitions of vibrationally excited formaldehyde in levels ν_4, $2\nu_4$, $3\nu_4$, ν_2, ν_3, and ν_6 are observed and effective vibrational temperatures for modes 2, 3, 4, and 6 are determined and discussed.

Introduction

Pyrolysis, which is the thermal decomposition of molecules in the absence of oxygen, has both scientific [1-16] and industrial [17-19] applications. In flash pyrolysis jet experiments, the molecules undergo thermal decomposition as they pass through the heated nozzle. The subsequent supersonic expansion into vacuum results in rotational cooling [3, 8, 11, 16] of the products that simplifies spectral assignment and improves the sensitivity of a rotational spectroscopy [1, 5] experiment. Isolated in a molecular beam, reactive molecules and radicals, that may be important in atmospheric or interstellar chemistry, or are intermediates in combustion or pyrolysis applications, become available for spectroscopic studies [1-15]. A version of the pyrolysis nozzle designed by Chen *et al* [2, 6] has become a

widely used instrument for laboratory studies of the products of pyrolysis reactions. Recently, the mechanisms of chemical reactions inside the flash pyrolysis reactor were investigated in the research group of G. B. Ellison. [13-15]

Quantifying concentrations of reaction products is important for understanding dynamics and kinetics in a pyrolysis reactor, but is also a challenging task. In the last decade there has been significant advances in quantifying photolysis [20-22] and pyrolysis [15] reaction products in a molecular beam using photoionization mass spectrometry (PIMS) that employs tunable VUV radiation from a synchrotron [23, 24]. The photoionization efficiency (PIE) dependence on the photon energy helps to distinguish between isomers and species with the same mass-to-charge ratio, which is not possible in PIMS experiments that use a fixed frequency laser for ionization. The universality of the tunable VUV PIMS method for chemical dynamics and kinetics studies depends on the availability of the reference PIE curves for each reaction product, which must be measured in carefully crafted experiments [25, 26]. Features that may complicate understanding and quantifying PIMS results are dissociative photoionization of neutral reaction products and photodissociation of ions. The availability of synchrotron beamline time must be considered as well. A promising alternative ionization method, strong-field ionization by femtosecond laser pulses, was recently demonstrated [27]. Although similar issues of photo-induced dissociation must be considered, the technique is conveniently lab-based.

Chirped-pulse Fourier transform microwave (CP-FTMW) spectroscopy, pioneered by Brooks Pate and coworkers [28-33] is transforming microwave spectroscopy and advancing into the millimeter-wave and THz regions [31, 33-35]. Spectral regions as broad as ~10 GHz are covered in a single chirped pulse with high resolution (~100 kHz) and meaningful relative transition intensities. Due to its ~1 part per million spectral resolution, pure rotational spectroscopy has exceptional precision for determining the structures of molecules and

radicals [36]. Chirped-pulse (CP) rotational spectroscopy retains the advantages of traditional narrowband rotational spectroscopy: unambiguous assignment of molecules and radicals, distinguishing conformers and even enantiomers [37], vibrational states, and fine and hyperfine states. The elegant study [38] of isomerization dynamics by Pate and coworkers is the first example of how the broadband feature of the chirped-pulse technique may be applied to studying chemistry. In their experiments, rotational transitions of two molecular conformers of cyclopropane carboxaldehyde, separated by several GHz, are detected simultaneously. As the conformers are laser-prepared in different "zero-order" vibrational states near the energy of the isomerization barrier, the observed rotational line intensity is being redistributed and shifted, reflecting the degree of mixing of the conformers' wavefunctions, or, equivalently, the rate of isomerization. Simultaneous and rapid acquisition of spectra extending over a broad spectral range is essential for the feasibility of these experiments. The traditional Balle-Flygare Fourier transform microwave spectrometer [5, 7, 39, 40], the most advanced pre-chirped-pulse microwave spectrometer, is intrinsically a narrow bandwidth instrument, which uses a high-Q cavity to achieve maximal signal-to-noise (S/N) ratio. The high-Q cavity must be mechanically adjusted to maintain the cavity enhancement of the microwave field, in order to scan successive ~1 MHz spectral intervals. Due to unavoidable fluctuations in experimental conditions, reliable comparisons of line intensities separated by several GHz in a scanning rotational experiment with sub-MHz resolution can be a challenging task.

In a CP experiment, the arbitrary waveform generator (AWG) generates microwave chirps that sweep the entire frequency range of interest in $\lesssim 1$ μs. Rotational transitions in molecules and radicals that fall into the chosen frequency range are polarized by the chirped pulse with a linear in time frequency sweep and undergo free induction decay (FID), which is digitized in the time-domain by the fast oscilloscope. The Fourier-image of the recorded FID

4

is the spectrum of the molecular sample in the entire region. All transitions are affected equally by possible shot-to-shot fluctuations introduced by a pulsed molecular beam source or by slow changes in experimental conditions. *Transitions that belong to multiple species can be recorded simultaneously with meaningful relative intensities and can be converted to branching of reaction products.*

Another fundamental advantage of CP spectrometers compared to a traditional narrow-band apparatus, is the more efficient excitation of rotational transitions by a chirped pulse when broad spectral ranges are considered.[28] Unlike with transform-limited (TL) single-frequency excitation, the bandwidth of a frequency-chirped excitation, Δv, is decoupled from its duration. For example, a $\Delta v = 10$ GHz chirp can have a duration of 1 μs (or longer), whereas a TL pulse of the same bandwidth must be as short as ~ 1 ns, thus severely limiting the amount of energy from that pulse that is available for polarizing molecular transitions. Treatment of fast passage excitation in the weak-field limit by McGurk *et al* [41, 42] [*Footnote*: for more discussion of this topic, see the Chapter by Shoemaker [43], CP papers by the Pate [28], Schnell [44] and Field [35] research groups, and the book by Akulin and Karlov [45] for an overview of semiclassical treatment of light-matter interactions], which is appropriate for most rotational CP experiments, shows that the induced polarization (and thus the FID signal strength) is proportional to $1/\sqrt{\Delta v}$ (Eq. 4), which is a more favorable scaling, especially for large bandwidth excitations, than the $1/\Delta v$ dependence with TL pulses. A remarkable illustration of the efficiency of chirped-pulse excitation combined with broadband detection is given by Dian *et al* [38]: in the coalescence experiment discussed above, measurements that took 52 hours using the CP-FTMW technique would require 27 years to complete with the traditional cavity-FTMW spectrometer! For the current status of the research with broadband CP spectroscopy, the

reader is referred to the recent review by M. Schnell [46] and the special issue of the Journal of Molecular Spectroscopy [47].

In the present work we introduce broadband chirped-pulse rotational spectroscopy for studies of dynamics and kinetics in a flash pyrolysis reactor. We demonstrate that chirped-pulse spectroscopy is a nearly universal tool for simultaneous and quantitative detection of multiple reaction products. The deduced product branching can be compared with results of computer modeling to attain an understanding of kinetics and dynamics of underlying chemical reactions. We optimized the excitation of multiple species by introducing the multi-chirp approach, in which a series of relatively narrowband chirps excite known molecular rotational transitions. The bandwidth of the chirps is reduced to take full advantage of the limited power of solid state amplifiers in the millimeter-wave range, but at the same time the bandwidth is made sufficiently broad for the excitation to remain in the weak-field limit and to avoid saturation. Excitation with multiple narrowband chirps thus achieves the optimal FID signal for the given hardware and permits a straightforward interpretation of the observed transition intensities.

In other series of experiments, which are described in this Perspective, broadband chirped excitation is utilized to locate rotational transitions that belong to vibrationally excited molecules. The intensities of those lines sample the vibrational population distribution in the molecules following adiabatic cooling in the jet, and are rationalized in terms of intramolecular energy flow induced by collisions with rare gas atoms. It is important that in both types of experiment, we apply broadband FID detection and obtain meaningful relative intensities of rotational transitions, which can be quantified to obtain reaction product branching and vibrational population distribution.

The approach of quantifying reaction product ratios, with isomer- and quantum state-selectivity, using CP rotational spectroscopy can be extended beyond studies of pyrolysis reactions. Detailed understanding of elementary chemical reactivity can be gained in a CP experiment, in which a chemical reaction is initiated by the laser excitation. The nascent vibrational population distribution in products of unimolecular photo-decomposition was recently observed in a CPmmW study and proposed as an additional tool for understanding the transition state(s) properties [48]. In such an experiment, a balance must be struck to ensure that there are sufficient post-photolysis collisions in the beam in order to equilibrate all product molecules at a lower rotational temperature, but not so many as would cause secondary reactions and would corrupt the nascent vibrational state distributions. Another approach could be to initiate and study complex chemistry in a cold beam. Experiments are under way in the Suits group to apply CP spectroscopy to dynamics and kinetics studies in a well-characterized pulsed uniform supersonic flow [49] obtained with the Laval nozzle.

Our choice of the millimeter-wave (mm-wave) spectral region for the present experiments is dictated by the type of chemistry we have chosen to study. When investigating the mechanisms of chemical reactions in relatively small organic molecules, it is often desirable to monitor small, two-heavy-atom products such as H_2CO, HNO, HCN, HNC, HCO, methoxy, HO_2, vinylidene [50], C_2H, and their isotopologues. In a cold ($T = 4$ K, $kT/hc = 3$ cm^{-1}) molecular beam, these molecules have their most intense $J = 1 - 0$ rotational transitions in the mm-wave region (60 – 100 GHz). Rotational transitions with $J = 4 - 3$ and $J = 7 - 6$ of larger, three- and four-heavy-atom molecules, such as CH_3CHO, CH_2CO and CH_3COCH_3, occur in this spectral region as well. Chirped-Pulse millimeter-Wave (CPmmW) spectroscopy, developed recently in the Field group [35, 48, 51, 52] as part of a collaboration with the Pate group, is an extension of the CP-FTMW technique to the mm-wave region. In the present paper we describe how the CPmmW spectrometer can be of transformative value

in studies of pyrolysis dynamics and kinetics, further enhanced by the multi-chirp scheme that is described here.

CPmmW pyrolysis experimental setup

The Chen nozzle was manufactured in the University of Colorado at Boulder machine shop and is a modified version of the nozzle used by the Ellison group [10]. Figure 1 shows the schematics of the nozzle and the spectrometer of the Field group CPmmW pyrolysis experiment. The 5.7 cm long, 1 mm inner diameter silicon carbide (SiC) tube (Saint-Gobain Ceramics, Hexoloy SE), the "tubular reactor", is inserted into a counterbore in the faceplate of the pulsed valve (General Valve, Series 9). Two carbon discs with Molybdenum electrodes connect the SiC tube to the electrical current supply that resistively heats the 3.2 cm section of the tube that is located between the two electrodes. The temperature of the outer wall of the SiC tube, which is indicative of (but not necessarily equal to) the temperature inside the reactor, is measured by an optical pyrometer (Leeds & Northrup 8632-C) in the $T_{\text{wall}} = 1000 - 1800$ K range. A water-cooled baffle provides support for the SiC tube and isolates the pulsed valve from thermal radiation emitted by the hot SiC tube. The gap between the baffle and the faceplate of the valve serves as an additional thermal isolation protecting the valve. At a 20 Hz gas pulse repetition rate and a stagnation pressure in the valve of $p_0 = 3$ bar, the pressure in the chamber, maintained by a 2400 ℓ/s turbomolecular pump (Osaka TG2400MBWC), is 2.5×10^{-5} mbar.

Ethyl nitrite was synthesized by adding hydrochloric acid to a solution of $NaNO_2$ (6 g) and ethanol (8 ml) in 25 ml of water. The ethyl nitrite vapor was condensed at -78 °C and then mixed with argon carrier gas in a sample cylinder. A mixture was made to contain 0.1% CH_3CH_2ONO and 99.9% Ar (by mole).
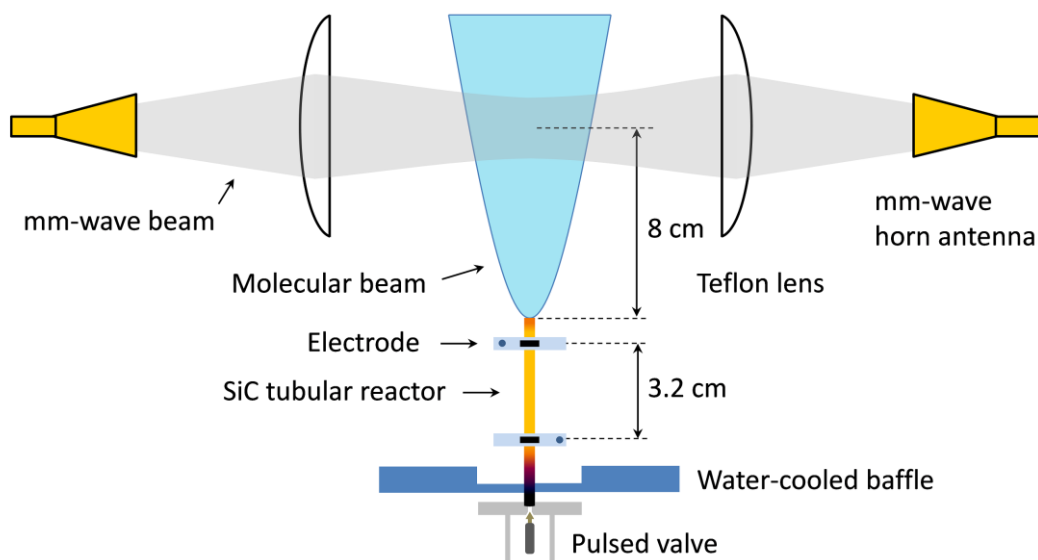
Figure 1. **Schematic of the experimental setup**. A pulsed valve and the attached SiC tube (tubular reactor) are mounted inside the vacuum chamber. The part of the reactor located between the two electrodes can be resistively heated to $T_{wall} = 1000 - 1800$ K. A water-cooled copper baffle disk isolates the valve from the hot part of the SiC tube. Precursor molecules entrained in a carrier gas are introduced to the tubular reactor where flash pyrolysis reactions take place. The reaction products emerge from the SiC reactor and expand supersonically into the vacuum chamber. The molecules are cooled during the adiabatic expansion to about 4 K rotational temperature and can be studied by rotational spectroscopy. The millimeter-wave beam of the CPmmW spectrometer, shaped by two Teflon lenses, crosses the gas jet in the collision-free region of the expansion.

The CPmmW spectrometer is described in detail by Park *et al* [35]. Here we provide an overview of the spectrometer with some modifications, and describe its adaptation to the flash pyrolysis source. The Tektronix AWG7082C arbitrary wave generator, operating at 8 Gsamples/s rate, forms chirped pulses that are mixed with a 10.7 GHz Miteq PLDRO fixed-frequency phase-locked oscillator. The resultant difference frequency is put through a bandpass filter, multiplied by 8 in an active multiplier chain with +13 dBm (20 mW) output power, and broadcast from a pyramidal horn antenna. A direct reading precision attenuator (60 dB maximum attenuation) is introduced between the multiplier chain and the horn antenna for intensity calibration purposes.

As shown in Fig. 1, a Teflon lens (50 cm focal length at 500 GHz, 15 cm diameter, custom constructed by Thorlabs) loosely focuses the millimeter-wave (mm-wave) beam to a 3 – 5 cm diameter spot at the center of the chamber, 8 cm downstream from the tip of the SiC tube, where it intercepts the molecular beam generated by the pyrolysis nozzle in its post-expansion collision-free zone. The molecular beam *is not skimmed* in order to maintain a total number of molecules in the mm-wave irradiated volume (~100 cm^3) that is optimal for our CPmmW experiment. The number density of HNO molecules (which corresponds to the spectrum shown in Fig. 3(d)) in that interaction region is about 10^{12} cm^{-3} (T_{wall} = 1500 K). A second Teflon lens and horn antenna collects the FID from molecules in the interaction region. The FID is then mixed with the 77.51 GHz mm-wave output of a phase-locked Gunn oscillator. The difference frequency is amplified by a low noise amplifier (Miteq AMF-7D-00101800-24-10P, 55 dB gain) and recorded by the Tektronix DPO70804C fast digital oscilloscope (8 GHz, 25 GSamples/s). In this experimental setup the Gunn oscillator is locked to the 8th harmonic of 9.6875 GHz, which is obtained by mixing the output of the second channel of the AWG, running continuously at a fixed frequency of 1.025 GHz, and the 10.7 GHz phase-locked oscillator that is simultaneously utilized by the upconversion arm of the spectrometer [33]. Using an AWG output allows choice of a downconversion mm-wave frequency that is conveniently situated with respect to the transitions of the molecular products. *Accurately maintaining the relative phases of the FIDs generated by successive chirped pulses is necessary for averaging.* We have determined that the phase-locked oscillators are the primary source of phase instability. To reduce their phase drift, the oscillators are water cooled to 15 ± 0.1 °C and isolated from lab air convection.

Multi-chirp technique

A major advance in the capabilities of the CPmmW spectrometer exploits the FastFrame™ technology, available in the newer models of Tektronix oscilloscopes, to collect multiple FIDs from a single gas pulse, thereby reducing acquisition time [31]. Pate and coworkers have emphasized [31] the advantages of using the FastFrame™ technology for recording each FID in the sequence without the necessity of averaging them into the "Summary Frame". The evolution of species populations due to transient processes can be followed by a CP spectrometer in such an acquisition mode.

In addition to multiple repetitions of a simple chirp, the FastFrame™ or an analogous technology may be utilized to produce a sequence of chirps (multi-chirp), with different center-frequencies and bandwidths, during a single molecular beam pulse. This is particularly useful in relatively sparse spectra of product species that have weak signals at known transition frequencies. In addition, a broadband spectrum can be helpful in the initial determination of the reaction product compositions. The multi-chirp approach then may be used to simultaneously obtain higher signal-to-noise ratio (S/N) spectra of several chosen species with meaningful relative intensities that can be converted into their relative concentrations. Since the acquired signal intensity is inversely proportional to the square root of the bandwidth, a bandwidth reduction from 7 GHz to 20 MHz results in an 18-fold signal intensity increase. This is the important point; *several narrowband chirps of different spectral content can be used sequentially within one composite chirped pulse sequence to probe multiple reaction product transitions.*

The capabilities of the multi-chirp strategy are illustrated here by a study of the pyrolysis of ethyl nitrite, CH_3CH_2ONO [16, 53-56], in which the H_2CO, CH_3CHO and HNO products are detected. Without providing a rigorous proof, we discuss the following reactions

that are likely to lead to the observed products (Fig. 2). The precursor CH_3CH_2ONO has a relatively weak O–NO bond (about 42 kcal/mol) that readily breaks inside the hot reactor to yield ethoxy, CH_3CH_2O, and NO radicals.[16, 54, 57] The ethoxy radicals undergo rapid decomposition to form either ($H_2CO + CH_3$) or ($CH_3CHO + H$) products.[16, 58, 59] The HNO product can be formed by either unimolecular decomposition of the precursor, the $CH_3CH_2ONO \rightarrow CH_3CHO + HNO$ reaction, or via H abstraction reactions by NO.
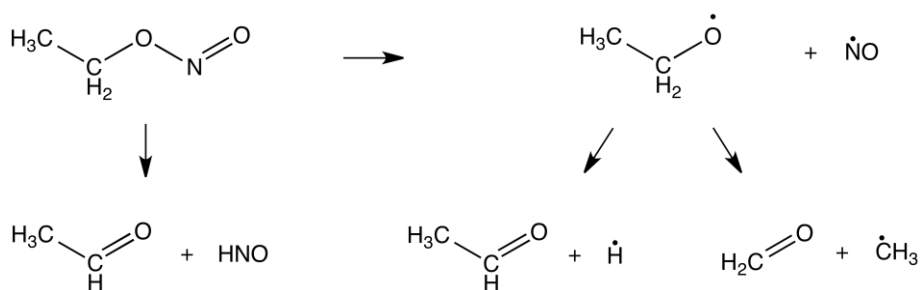

Figure 2. Suggested primary reactions in pyrolysis of ethyl nitrite. CH_3CH_2ONO can undergo single bond fission and decompose to CH_3CH_2O and NO radicals [16, 54, 57], after which the ethoxy radical rapidly follows one of the dissociation channels [16, 58, 59]: to form the H_2CO and H, or CH_3CHO and H products. Alternatively, the precursor CH_3CH_2ONO may undergo unimolecular decomposition to CH_3CHO and HNO. Possible secondary reactions are not considered here, but may influence the measured concentrations.

Figure 3 (a) displays a sequence of 22 chirps that is comprised of two kinds of narrowband chirps, each of them targeting a particular product, CH_3CHO and HNO, and a broadband (BB) chirp, which provides an overview of all possible products, including H_2CO. The chirps are separated by 10 μs time intervals and the entire 220 μs sequence overlaps in time with the ~ 500 μs long gas pulse that contains the pyrolysis products. To ensure a uniform sampling of the earlier and the later portions of the gas pulse, the AWG is setup to alternate the kinds of chirps: the pattern $1 \times BB + 3 \times CH_3CHO + 3 \times HNO$ is repeated three times followed by an additional BB chirp that completes the sequence (Fig. 3(a)).

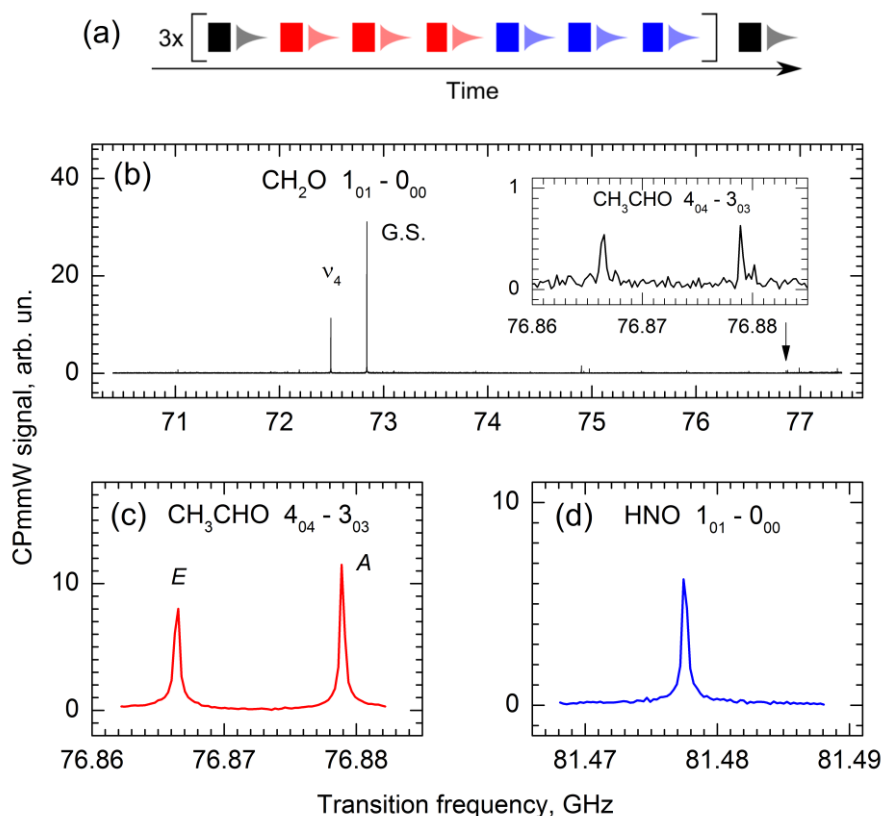Figure 3. CPmmW spectroscopy of CH_3CHO, H_2CO, and HNO products of CH_3CH_3ONO pyrolysis using the multi-chirp approach. (a) Example of a multi-chirp sequence. In this sequence, a broadband 7 GHz chirp covering 70.4–77.4 GHz (black) is used in combination with 20 MHz chirps centered on relevant known transitions for CH_3CHO [60, 61] (red) and HNO [61, 62] (blue) to study pyrolysis of ethyl nitrite. (b-d) Spectra obtained from use of the chirp sequence in (a). Rotational J_{KaKc} assignments of the transitions are provided. (b) The broadband chirp, covering 70.4–77.4 GHz, provides an overview of the possible products and contains transitions of formaldehyde in the vibrational ground state (G.S.) and in the ν_4 excited state. The insert magnifies the spectral region that contains two acetaldehyde transitions. (c) The narrowband chirp covering the 76.862–76.882 GHz region with the two acetaldehyde transitions that belong to the E and A symmetry ground states of the internal rotor excitation [60, 61]. (d) The narrowband chirp covering the 81.468 – 81.488 GHz region with the HNO transition [61, 62].

Recording and averaging the FIDs in the multi-chirp scheme requires some additional data processing. In this work, a sequence of 4 μs long FIDs that follow each of the 22 chirps is recorded into the fast memory of the Tektronix oscilloscope operating in the FastFrame™ mode. The 50 ms interval between the gas pulses (@ 20 Hz) provides time to transfer that FID sequence from the fast memory to the main memory of the oscilloscope, where it is stored to be averaged, each FID separately, with the sequence of FIDs that result from the next gas pulse. In the example shown in Fig. 3 we have averaged over 10,000 gas pulses,

13

which takes about 10 minutes. Averaging of up to 200,000 gas pulses (3 hours) is practical and has been used to detect weaker signals. After the experiment is completed, the file containing the sequence of 22 averaged FIDs is transferred to a personal computer where the FIDs from each *kind* of chirp are additionally averaged with each other. The resulting three time-domain FIDs are Fourier-transformed to obtain the frequency-domain spectra shown in Fig. 3(b-d).

In some instances it may be useful to omit the last averaging step and convert each FID in the sequence to a frequency domain spectrum [31]. As mentioned before, this approach can be used to monitor transient processes. We have converted each of the 22 FIDs to spectra and examined the time evolution of the spectral line intensities. The vibrational temperature of H_2CO, gauged by its ν_4 state effective temperature (see below), decreases slightly toward the end of the 220 μs portion of the gas pulse. One of a few possible explanations for that is that the SiC tube is cooled by the fast passage of the gas pulse. In this work we are not focusing on modeling the gas flow in the reactor and take advantage of averaging FIDs of the same kind from all parts of the multi-chirp sequence. It is important to note that, for best S/N, averaging in the time-domain followed by Fourier-transformation is superior to Fourier-transformation of the individual FIDs with subsequent averaging in the frequency-domain.

The bandwidth of chirps of a particular kind and their repetition frequency in the sequence can be chosen to attain comparable S/N for all pyrolysis products; thus re-allocation of the spectrometer's sensitivity between transitions with different intensities is implemented. This multi-chirp scheme further improves the ability of the chirped-pulse technique to simultaneously detect multiple species and to quantify the branching between reaction products. Finally, the chirps may contain frequencies situated both above and below the frequency of the mm-wave local oscillator (77.51 GHz in this experiment) that is used for

14

down-conversion. The HNO line in the 81.468 – 81.488 GHz region and the broadband spectrum of the 70.4 – 77.4 GHz region span more than 11 GHz, yet are obtained using an 8 GHz bandwidth oscilloscope. Aside from the ~200 MHz dead region near the down-conversion frequency, this method effectively doubles the oscilloscope-limited bandwidth available for FID detection.

A noteworthy feature of these spectra is that some species are detected solely from the broadband chirps, namely the formaldehyde product and the remaining ethyl nitrite parent species. Acetaldehyde transitions can also be detected, albeit with S/N of only 4:1 (Fig. 3(b), insert). If the entire chirp sequence consisted of broadband chirps, this acetaldehyde S/N would increase to 19:1. However, excitation of these acetaldehyde transitions by the narrowband chirps of the sequence illustrated by Fig. 3(a) results in the acetaldehyde spectrum (Fig. 3(c)) that has a S/N approaching 100:1. Similarly, the narrowband HNO chirps achieve the high S/N ratio of a known transition (Fig. 3(d)). While the transitions in this example are all sufficiently intense to be detected using broadband chirps, the power of the multi-chirp technique is demonstrated for future detection of transitions of products from minor reaction channels or with weak transition moments.

Rotational temperature

Determination of rotational temperatures is crucial for determining the relative species concentrations in a CPmmW experiment [48]. We use the ratio of intensities of the $J_{KaKc} = 4_{04}$ $- 3_{03}$ transitions to the sum of the $4_{23} - 3_{22}$ and $4_{22} - 3_{21}$ transition intensities in acetaldehyde molecules as a thermometer. The line intensities were corrected for the frequency-dependent profile of the chirp obtained with 40 dB attenuation of the $\times 8$ active frequency multiplier, and matched by a PGOPHER [56] simulation. Acetaldehyde, which is a *reaction product* of ethyl

nitrite pyrolysis, was measured using a chirp sequence that contains the broadband chirps exclusively. Despite the high temperatures in the pyrolysis nozzle, we measure very low rotational temperatures (T_{rot}) of acetaldehyde close to those typically found in supersonic expansions. We find that $T_{rot} = 4 \pm 1$ K at $T_{wall} = 1000 - 1800$ K. There is no detectable difference in T_{rot} when acetaldehyde of 0.1% mole fraction entrained in argon is expanded from the heated pyrolysis nozzle. At room temperature, $T_{wall} = 300$ K, acetaldehyde has $T_{rot} = 3.5$ K. We conclude that molecular rotations of acetaldehyde expanded from this heated Chen nozzle are effectively thermalized to the translational temperature of the carrier gas. This conclusion is consistent with the consensus in the literature [63] that rotational degrees of freedom are cooled efficiently in the supersonic expansion. Indeed, the typical translational temperature of the carrier gas of several Kelvins is close to the energy spacing between the rotational levels of most molecules and efficient relaxation of highly excited rotational levels is possible. We assume that all pyrolysis products thermalize to similar values of T_{rot}. It is possible, however, that some reactions will result in products with anomalously high rotational excitation. Excess rotational energy may remain in those products, compared to other molecules, even after cooling in the supersonic expansion. The rotational temperature issues are all soluble, once the frequency region covered by the spectrometer is extended, and more than one rotational transition in each product is detected. For example, in the $140 - 150$ GHz region formaldehyde molecules have both their $J = 2 - 1$, $K = 0$ transition and two $J = 2 - 1$, $K = 1$ transitions. Assuming that the J- and K- rotational temperatures are equal, direct measurement of the rotational temperature of formaldehyde and other small, two-heavy-atom, molecules is possible in the $110 - 170$ GHz region. Larger molecules, such as acetaldehyde, have their $K = 0, 1, 2, 3$ transitions in either the present or the extended frequency range configuration. In principle, it is possible to measure several $(J + 1) - J$ transitions to deduce the rotational temperature. However, great care should be taken in calibrating and comparing

the line intensities that are spread sufficiently far to require swapping the microwave or the mm-wave components in the spectrometer to measure those lines. An important factor to be considered when choosing the spectral range for the spectrometer is the Boltzmann maximum of the Δn_0 at a given ambient temperature. [31]

Vibrational temperature

Vibrations are known to be generally more resistant to thermalization in the supersonic expansion than rotational excitations [64-67]. CPmmW spectroscopy makes it possible to detect rotational transitions, with meaningful relative intensities, that belong to molecules in different vibrational levels [48]. Thus, the vibrational population distribution (VPD) can be inferred. In the present work we compare the VPDs of OCS, H_2CO, and CH_3CHO molecules that exit the pyrolysis nozzle. They illustrate the unique use of rotational spectroscopy as a measure of vibrational populations.

OCS

By expanding the mixture of 3% OCS in argon from the heated reactor we have observed the $J = 6 - 5$ rotational transitions [68] that belong to the following vibrational states of OCS: (1, 0, 0), (1, 1^{1e}, 0), (1, 1^{1f}, 0), G.S., (0, 1^{1e}, 0), (0, 1^{1f}, 0), (0, 2^0, 0), and two pairs of rotationally unresolved vibrational states (0, 2^{2e}, 0), (0, 2^{2f}, 0), and (1, 3^{3e}, 0), (1, 3^{3f}, 0). The vibrational quantum numbers are designated (v_1, v_2^ℓ, v_3), with v_1 representing the C=S stretch (866 cm^{-1}), v_2 the bend (520 cm^{-1}), v_3 the C=O stretch (2072 cm^{-1}), and ℓ the vibrational angular momentum [36, 69]. Here we adopt a multi-temperature model [70] in which the vibrational temperature of an individual level v is defined as

$$T_v = E_v / \ln\left(\frac{g(v)S_{GS}}{g(GS)S_v}\right) \qquad (1)$$

where S_v and S_{GS} are the measured rotational line intensity of the state v and the ground state, respectively, $g(v)$ and $g(GS)$ are the degeneracies, and E_v is its vibrational energy (in Kelvin). The sensitivity and the dynamic range of the spectrometer permits detection of the vibrationally excited OCS not only after the molecules are flash-heated in the reactor, but also in an experiment in which the SiC tube is kept at room temperature. In the latter measurement the vibrationally excited levels are less populated and the corresponding rotational line intensities, S_v, are smaller, if measured against the ground state line intensity, S_{GS}. In the following discussion we shall use vibrational temperatures divided by the temperature of the reactor wall, T_{wall}, as such a representation will help to relate the observed VPDs to the mechanisms of heating molecular vibrational degrees of freedom up to the T_{wall} and cooling them down to the expanding beam temperatures. In OCS, we found the VPD to be mostly Boltzmann, i.e. with the measured T_v for all vibrational levels to be approximately equal to a common vibrational temperature, T_{vib}, of the molecule.

The vibrational temperature T_{vib} of the OCS molecules expanded from the room temperature reactor has the ratio T_{vib} / $T_{wall} \approx 0.84$ in good agreement with the previous molecular beam studies by DeLeon and Muenter [66]. $T_{wall} = 300$ K is a special case in which molecular vibrations are *a priori* thermalized at T_{wall} temperature, and the small deviation of T_{vib} / T_{wall} from unity should be explained by the (slow) cooling of vibrations in the supersonic expansion. However, upon passage through the heated Chen reactor at $T_{wall} = 1500$ K, the ratio decreased to T_{vib} / $T_{wall} \approx 0.32$. The decrease in relative vibrational temperature can be rationalized by invoking either an unexpectedly efficient V – T/R cooling of molecular vibrations upon expansion from a $T_{wall} = 1000 – 1500$ K reactor, by allowing for

incomplete thermalization of the OCS molecules in the heated reactor during the ~100 μs residence time, or by a more complex scenario.

Vibrational energy transfer in OCS molecules has been studied extensively in the past [67, 71-74]. The equation

$$\frac{dT_{vib}}{dt} = -\frac{1}{\tau}(T_{vib} - T_{tr}) \qquad (2)$$

where τ, the time constant of the collisionally-induced V–T energy transfer, governs the vibrational temperature equilibration rate, and is applicable to the two cases in which the ambient translational temperature T_{tr} is above or below the T_{vib} [67]. We adopt the latter measured value of $1/(\tau p)$= 490 Torr^{-1} s^{-1} [67] to obtain $\tau = 5$ μs for T–V energy transfer between OCS molecules and argon atoms inside the heated reactor, where we estimate the average pressure to be $p = 0.5$ bar. The τ was measured in a fluorescence experiment in which excited vibrational levels of OCS were relaxed by collisions with Ar atoms in a room temperature cell [67]. Because the energy gap between the vibrations of OCS and the kinetic energy of argon atoms at 300 K or at 1500 K is similar, we believe that the τ value is valid for our pyrolysis conditions. It is clear from integrating Eq. (2) [67] and using the $\tau = 5$ μs value, that *vibrational thermalization of molecules in the hot reactor is fast* relative to the ~100 μs time-scale [14, 15] of residence time. For example, flash-heating room temperature OCS molecules mixed with Ar in a $T_{wall} = T_{tr} = 1500$ K reactor, requires 1 μs to reach $T_{vib} = 480$ K, and 13 μs to reach $T_{vib} = 1400$ K.

These estimates lead us to believe that the reduced T_{vib} / $T_{wall} \approx 0.32$ ($T_{vib} = 480$ K at $T_{wall} = 1500$ K) observed for OCS molecules can be explained either by accelerated V–T cooling in this pyrolysis experiment at elevated temperatures, or, what seems more plausible, by a more complex temperature distribution in the reactor. In the concluding section of this Perspective we present some evidence for the latter possibility and consider a multi-

component flow through the reactor. In that picture, it is only the layer of gas adjacent to the wall that is thermalized at the T_{wall} temperature, while molecules flowing closer to the middle of the tube are heated to lower (vibrational) temperatures.

H2CO

In formaldehyde, that is produced by pyrolysis of ethyl nitrite, the strong satellite line in the spectrum in Fig. 3 belongs to H_2CO molecules with one quantum of the ν_4 out-of-plane bending excitation [75].

Vibrational level	$3\nu_4$	$2\nu_4$	ν_2	ν_4	ν_6	G.S.	ν_3
$1_{01} - 1_{00}$ rotational frequency, MHz	71916.91 ± 0.20	72190.30 ± 0.20	72348.34 ± 0.20	72492.35 ± 0.05	72727 ± 1	72837.94 ± 0.05	73062 ± 1
Vibrational energy, cm^{-1} [75]	3480.7	2327.5	1746.1	1167.4	1249.6	0	1500.2

Table 1. Rotational $1_{01} - 1_{00}$ transition frequencies of H_2CO molecules in various vibrational levels measured in this work. A more precise value for the ground state transition of 72837.948 ± 0.01 MHz is available [76]. Transitions in levels ν_2, ν_4, ν_3 and ν_6 were previously measured by mm-wave experiments [77] (note the difference in mode notation), and the transition frequency in the $2\nu_4$ level is in agreement with the FTIR study [78]. The $3\nu_4$ level assignment was made based on its measured effective vibrational temperature (see Fig. 4 and text below). States ν_1 (2782.2 cm^{-1}) and ν_5 (2843.0 cm^{-1}) were not observed in this work.

Although this strong transition may be encoding information about the transition state through which the parent molecule has passed upon dissociation, we find that the VPD in this experiment has been strongly affected by collisional relaxation during the expansion. In fact, the ν_4 level population observed in formaldehyde, which results from a pyrolysis reaction (Fig. 3), is similar to the ν_4 level population in formaldehyde co-expanded through the heated pyrolysis reactor with argon or helium. Here we use the VPD of the latter measurement to characterize the vibrational relaxation dynamics of H_2CO molecules.

We assign several lines in the rotational spectrum of formaldehyde (not shown here) to vibrationally excited states of formaldehyde (Table 1). The effective vibrational temperatures (Fig. 4) of the five excited vibrational states are deduced from the observed line intensities in a way similar to that for OCS, but with a correction for the nuclear spin degeneracy in H_2CO. Due to the nuclear spin statistics of the two hydrogen atoms in the molecule, the antisymmetric vibrational levels (v_4 = odd) with even-K_a belong to the $I = 1$ total nuclear spin species, *ortho*-H_2CO, and the symmetric (v_4 = even) levels with even-K_a belong to the $I = 0$ species, *para*-H_2CO. All H_2CO molecules sampled by the $J_{KaKc} = 1_{01} - 0_{00}$ transition are in the $K_a = 0$ state, and are either *ortho-* or *para-* species depending on the symmetry of their vibrational state. The nuclear spin degeneracies are $g(v_4)$=3, $g(2v_4)$=1, $g(3v_4)$=3, and $g(v_6)$=3, $g(v_2)$=1, $g(v_3)$=1. Therefore, for example, we divide the intensity of the $J_{KaKc} = 1_{01} - 0_{00}$ transition in the v_4 state by 3 when deriving the effective vibrational temperature.

We measured the T_v / T_{wall} ratio for the v_4 level of H_2CO at different reactor temperatures. The population of the v_4 level was in near equilibrium with the reactor at room temperature: T_v / T_{wall} = 0.85. The relative effective vibrational temperature T_v / T_{wall} was measured to be 0.47, 0.57 and 0.63 at T_{wall} = 1150 K, 1500 K and 1750 K, respectively, in argon, and 0.9 at T_{wall} = 1500 K in helium.
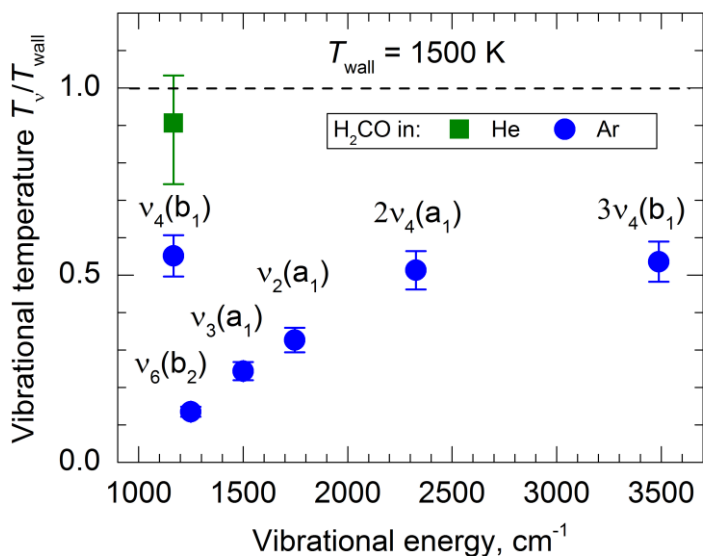
Figure 4. The T_v / T_{wall} ratio measured for formaldehyde in vibrational states ν_4, $2\nu_4$, $3\nu_4$, ν_2, ν_3, and ν_6. The symmetries of the corresponding vibrational wavefunctions are given in the parentheses. Formaldehyde molecules were mixed with the carrier gas (argon or helium) and expanded through the tubular reactor heated to $T_{wall} = 1500$ K. The horizontal axis is the vibrational excitation energy of each state [75]. The vibrational population distribution is non-Boltzmann with the mode ν_4 showing the largest relative population.

Unlike OCS, for which all its states would fall on a straight horizontal line in a plot similar to Fig. 4, H_2CO exhibits different vibrational temperatures for different vibrational levels. The data in Fig. 4, which correspond to the ν_4 state (out-of-plane bend) and its $2\nu_4$ overtone have effective vibrational temperatures of $T_v = 750 - 900$ K, displaying the largest relative population compared to levels ν_6 (in-plane bend), ν_3 (sym. CH_2 bend) and ν_2 (C–O stretch). The rotational transition at 71916.91 MHz (Table 1) is assigned to the $3\nu_4$ overtone (and not to $2\nu_2$) because its T_v matches the effective temperature of other states with quanta in mode ν_4.

We invoke Coriolis-type interactions between the vibrational levels of formaldehyde [75, 79, 80] to account for the observed non-Boltzmann VPD in formaldehyde. The Coriolis

interaction matrix element that couples the vibrational states ν_4 and ν_6 through the a-axis rotation [80]

$$< v_4 = 1, v_6 = 0, J, K_a| \, H_{Cor} \, |v_4 = 0, v_6 = 1, J, K_a > = i\xi_{46}^a K_a \qquad (3)$$

is proportional to the projection of the total angular momentum J on the a-axis, K_a, and the Coriolis coefficient ξ_{46}^a. When the nozzle is heated and high values of J, K_a are populated, facile mixing and thermalization of vibrational states occurs [79]. Upon collisional cooling in the supersonic expansion, the vibrational state populations in ν_4 and ν_6 levels redistribute, mediated by the strong Coriolis interaction between these two levels, following the ambient temperature of the molecular beam. Eventually the Coriolis interaction between the pair of vibrational states shuts down at low J, K_a and locks in the VPD. It is this final population distribution that we observe in the collisionless region of the beam.

The measured ratio of line intensities for ν_4 and ν_6 levels is 1200 and the energy gap between these levels is 82 cm^{-1}. An effective temperature of this two-level system (TLS) can be calculated, using Eq. (1), to be 82/ln(1200) = 12 cm^{-1} = 17 K (both levels are $g(\nu)=3$ degenerate). Assuming that this is a TLS that is isolated from other vibrational levels (which is probably a good assumption since the $\nu_6 \leftrightarrow \nu_4$ Coriolis interaction is the strongest of all), but has good thermalization with Ar atoms in the beam, the $T = 17$ K must be indicative of the ambient temperature at which the ν_6, ν_4 vibrational level population froze. Since the a-axis rotational constant of formaldehyde is 9.4 cm^{-1}, the Coriolis $\nu_6 \leftrightarrow \nu_4$ energy transfer at $T = 17$ K is facilitated by a rotational excitation as small as $K_a = 1$. Other levels are connected by Coriolis coefficients that are significantly smaller than ξ_{46}^a, or $\xi_{2\times4,4+6}^a$, $\xi_{4+6,2\times6}^a$, etc. [80] and the population flow between them terminates at higher temperatures. Thus most vibrational population is accumulated in the ν_4, $2\nu_4$ and $3\nu_4$ levels of formaldehyde, which results in their highest effective vibrational temperatures (Fig. 4).

The symmetry of the formaldehyde molecule may contribute to the immunity of mode v_4 to collisional V–T/R relaxation. Exchanging the two hydrogen atoms by a C_2 operation will leave the total wavefunction of the H_2CO molecule unchanged if v_4 is even and will change its sign if v_4 is odd, given that K_a is even. Since interconversion between the *para-* and *ortho-* species is slow on the time-scale of the experiment, relaxation with $\Delta v_4 = 1$ must be accompanied by a $\Delta K_a = 1, 3, \ldots$ transition. This concerted ($\Delta v_4 = 1$, $\Delta K_a = 1, 3, \ldots$) collisionally-induced transition is likely to have small cross section.

CH₃CHO

In order to evaluate the VPD in CH_3CHO molecules, the frequencies of the rotational transitions of acetaldehyde are calculated.

Vibr. mode	Approx. mode [81]	Vibrational energy, cm^{-1} [81, 82]	Vibrational corrections to rotational constants, MHz		
			α^A	α^B	α^C
15	CH₃ torsion	143.8	434.007	-5.88120	-21.8340
10	C=O s bend	508.8	-595.041	-1.30977	15.2360
14	CH₃ rock	764.1	101.024	16.9212	-4.38293
9	C–C s str	865.9	-60.1893	33.9728	41.7420
13	CH a bend	1097.8	54269.4	146.372	31.4347
8	CH₃ rock	1113.8	-54189.2	-84.5799	2.68258
7	CH₃ s bend	1352.6	134.596	45.6772	53.2273
6	CH s bend	1394.9	204.392	-32.5285	6.44373
5	CH₃ a bend	1433.5	4086.87	29.0212	-51.4157
12	CH₃ a bend	1438.3	-4127.68	-81.8807	-5.32976
4	C=O str	1746	268.361	31.0598	33.2728
3	CH str	2715.4	89.2801	10.2636	8.91806
2	CH₃ a str	2921.5	188.013	6.17035	3.06319
11	CH₃ a str	2964.3	132.875	6.64735	5.56099
1	CH₃ a str	3014.3	161.561	4.07640	5.23577

Table 2. Calculated vibrational corrections to the rotational constants of acetaldehyde.

Vibration-rotation constants α^A, α^B, and α^C (Table 2) that describe the changes in rotational constants upon vibrational excitation [83] were calculated in the coupled-cluster approximation known as CCSD(T) [84], using the ANO1 contraction [85] of the atomic natural orbital basis sets of Taylor and Almlöf [86]. These constants require computation of the harmonic and cubic force fields, the details of which are fully described in Ref. [87]. The ANO1 basis set together with the CCSD(T) treatment of electron correlation is known to give a very good estimate of fundamental vibrational frequencies (an accuracy of *ca.* 10 cm^{-1}); the present results suggest that it is also quite accurate for estimation of rotation-vibration interactions, at least in cases where Coriolis resonance effects are not significant.

Acetaldehyde molecules were found to be vibrationally cold. No rotational transitions in vibrationally excited levels of acetaldehyde were found in the $\pm$ 2 GHz spectral range around the $4_{04} - 3_{03}$ transition of the vibrational ground state molecules. We attribute the existence of such highly efficient vibrational cooling in acetaldehyde to the internal CH$_3$ rotor, with its 143 cm^{-1} rotor frequency [81, 82], which may facilitate energy transfer between excited vibrational levels and the translational motion of the cold carrier gas [88].

Product branching

Measurement of the relative concentrations of different pyrolysis reaction products is possible using the CPmmW technique. The input parameters are: 1) the integrated intensities of the observed and assigned transitions, 2) their electric (transition) dipole moments, 3) the rotational temperature(s) of the corresponding species and 4) the parameters that describe the excitation chirped pulse(s). In the weak field limit, fast passage excitation [44] can be implemented and the observed signal, *S,* is described by the following equation [28, 35, 41]

$$S \propto \frac{\Delta n_0 E_0 \mu^2}{\sqrt{\alpha}} \qquad (4)$$

where Δn_0 is the initial population difference of the two rotational levels between which coherence is created by the mm-wave field with amplitude E_0. The electric (transition) dipole moment, μ, and the chirp-rate, defined, for a linear frequency sweep over the frequency range $\Delta \nu$ in time τ as $\alpha = \frac{\Delta \nu}{\tau}$, are the other two relevant parameters. The condition for weak field excitation [35],

$$\frac{\Omega_R}{\sqrt{\alpha}} \ll 1, \qquad (5)$$

where $\Omega = \frac{\mu E_0}{h}$ is the Rabi frequency, implies weak coupling of the molecular transitions to the mm-wave field. An additional, to Eq. (5), requirement for fast passage is that the chirp sweeps through its frequency range more rapidly than decoherence effects can cause the oscillating molecular dipoles to evolve out of phase with each other. In this experiment the leading source of dephasing is the Doppler effect due to divergence of the molecular beam. This Doppler dephasing becomes significant on a $3 - 5 \, \mu$s timescale, and the chirp durations are programmed to be $1 \, \mu$s.

Whether the condition in Eq. (5) for weak field excitation is fulfilled can be verified by evaluating the electric field amplitude, E_0, in the interaction region, and thus the Rabi frequency. Although the power of the mm-wave source is known and can be converted to the E-field amplitude, a more precise determination of the E-field strength is achieved by directly observing the response of the molecular or atomic sample to the mm-wave excitation by using the CPmmW spectrometer [35, 51]. In this work we excite the $8_{17} - 8_{08}$ rotational transition in SO_2 molecules, expanded from the (cold) pyrolysis nozzle, with single frequency, $4 \, \mu$s long pulses. The Rabi frequency of $\Omega_R(SO_2) = \frac{\mu E_0}{h} = 0.45$ MHz and the E_0 = 8.8 V/m were determined by measuring the period of the FID beats against the E-field of

the excitation pulse (nutations).[51] The measured E-field amplitude of $E_0 = 8.8$ V/m is the same for chirped excitation, and the validity of condition of Eq. (5) can be verified. For the CH_3CHO $4_{04} - 3_{03}$ transitions ($\mu_a = 2.42$ D [60]) polarized by a $\Delta v = 20$ MHz, $\tau = 1$ μs chirp the Rabi frequency is $\Omega_R(CH_3CHO) = \frac{\mu E_0}{h} = 0.67$ MHz and $\frac{\Omega_{R(CH_3CHO)}}{\sqrt{\alpha}} \approx 0.15$. Agreement between the CH_3CHO line intensities obtained with the broad and the narrow chirps, as discussed above, is an additional confirmation that the narrowband $\Delta v = 20$ MHz chirped excitation does not drive the rotational transitions outside the linear region of the Rabi cycle and that Eq. (4) can be used to measure species concentrations and reaction branching ratios. These estimates are also consistent, when $\frac{\Omega_R}{\sqrt{\alpha}}$ is rescaled, with the saturation measurements of OCS transitions by Zaleski *et al* [29] that they have employed to establish the chirp bandwidths at which Eq. (4) is valid. Finally, it may be instructive to rewrite Eq. (4) in the form $S \propto \frac{\Omega_R}{\sqrt{\alpha}} \Delta n_0 \mu$. The physical meaning of the $\frac{\Omega_R}{\sqrt{\alpha}}$ term is the degree of polarization acquired by each molecular oscillator, and the $\Delta n_0 \mu$ term corresponds to the macroscopic polarization, which is proportional to the FID, of a sample of completely polarized oscillators [35, 41, 51].

In order to obtain the relative concentrations, the line intensities are normalized to account for the bandwidth of the chirps and for the frequency-dependence of the output power of the active multiplier chain. The dipole moments are usually known or can be calculated with sufficient precision. We employ the PGOPHER [56] program to simulate the rotational spectrum of several species at a specified rotational temperature. As discussed above, we use acetaldehyde as a thermometer molecule and assume rotational thermalization of all parent and fragment molecules to the common $T_{rot} = 4$ K. The relative species concentrations are varied in the PGOPHER program to match the relative line intensities of the simulation and the calibrated experimental spectrum.

To relate the concentrations of these products to the initial concentration of the precursor, a 0.1% mixture of acetaldehyde in argon was expanded from the nozzle at $T_{wall} =$ 1500 K. This signal corresponds to what would be a 100% conversion from ethyl nitrite to acetaldehyde, and can serve as a reference. For CH_3CH_2ONO pyrolysis at $T_{wall} = 1500$ K we obtain the $CH_3CHO : H_2CO : HNO$ product branching to be 21 : 2.8 : 1.1, where 100 corresponds to the concentration of CH_3CH_2ONO prior to pyrolysis. Thus, the overall conversion to these three products at $T_{wall} = 1500$ K is about 25%.

The temperature and pressure distributions in the pyrolysis reactor are not well characterized at the moment. Several experimental facts point to the possibility that there are concentric layers of flow in the reactor that do not mix completely with each other and have different temperatures. The most convincing evidence for that is that decomposition of methyl nitrite, CH_3ONO, carried out at the same experimental conditions as ethyl nitrite pyrolysis, is incomplete. In another experiment conducted at the same ($T_{wall} = 1500$ K) conditions, products that require cleavage of a 85 kcal/mol CH_3–CHO bond in acetaldehyde [89] are observed. Simple estimates based on the Arrhenius coefficients for these reactions show that for the 100 μs residence time in the reactor, the former observation requires the reactor temperature to be below 800 K, and the latter reaction turns on at or above 1500 K. The multi-layer structure of the flow in the reactor would be consistent with the behavior of the T_v / T_{wall} in OCS molecules. At $T_{wall} = 1500$ K there may be a center flow region where the OCS/Ar mixture is not heated to the T_{wall} during the flash through the SiC tube. The vibrational temperature averaged over all OCS molecules in the flow thus would be noticeably lower than the T_{wall}, $T_v / T_{wall} < 1$, which is observed in the experiment. However, when expanding through a room temperature reactor, the flow is at 300 K everywhere in the tube and $T_v / T_{wall} \approx 1$ in accordance with ours and previous [66] observations. These considerations imply fast thermalization of vibrational levels to the ambient temperature, in

accordance with our estimates for OCS in Ar (see the "Vibrational temperature" section). In formaldehyde (Fig. 4), the higher temperature of the ν_4 level in He carrier gas can be explained by more uniform heating of H_2CO molecules in the reactor because of faster diffusion of He compared to Ar.[90] Recent computational fluid dynamics simulation [14, 15] of a continuous flow tubular reactor indicates that the flow near the axis of the SiC tube is colder than that near the wall of the tube. Thus the incomplete, 25%, conversion of ethyl nitrite precursor into the three products may be explained by its incomplete thermal dissociation in the cooler core of the flow through the reactor. Another species that is identified in the spectrum in Fig. 3(b) is ethanol. However, ethanol is also found in the spectrum with the room temperature reactor and is likely to be a by-product of ethyl nitrite synthesis [54].

The uncertainty in the species concentrations measurement results from several sources: i) possible deviation of the rotational temperature of a product from that of the thermometer molecule (see "Rotational temperature" section), ii) the frequency-dependent intensity fluctuations observed in the transmitted chirps, likely to be caused by standing waves, iii) frequency-dependent non-linearity of the microwave and the mm-wave components' response in the 0 – 40 dB range of mm-wave attenuation set by the direct reading attenuator, iv) uncertainty in measuring the T_{rot} introduced by ii) and iii), and v) molecules in vibrationally excited states for which rotational transitions are not assigned and thus are not included in the line intensity calculation. We estimate that ii) – v) account for an uncertainty of ± 30% in the relative concentration measurements. The limitation i) is perhaps the most fundamental one in this experiment. Although there is a reason to believe that cooling in the beam equilibrates rotational degrees of freedom of most of the molecules very effectively, the validity of this assumption requires further investigation.

Conclusions

We have demonstrated the feasibility and some advantages of chirped-pulse rotational spectroscopy to quantify reaction product branching and quantum state population distributions in product molecules. As an example, we have observed the flash pyrolysis of ethyl nitrite and measured its decomposition yields of H_2CO, CH_3CHO, and HNO. Studies in the 60 – 100 GHz millimeter-wave spectral region are capable of sampling the populations of most polar two-heavy-atom molecules as well as larger molecules. A multi-chirp modification of the CPmmW experiment is demonstrated to be a useful approach to CP studies. Chirp segments with different independently chosen spectral content form a sequence that covers a single gas pulse. The number of chirps of each kind in the sequence and their bandwidth can be varied to achieve the desired S/N in each spectral region/species targeted. In this way the sensitivity of the spectrometer can be effectively re-distributed between the reaction products with different abundances and electric dipole moments.

From the CPmmW spectra we find that rotations of acetaldehyde molecules are effectively cooled to $T_{rot} = 4 \pm 1$ K by the supersonic expansion even at the elevated temperatures of the pyrolysis reactor. State-specific vibrational temperatures in OCS, H_2CO, and CH_3CHO molecules were measured by analyzing the intensities of rotational transitions of molecules in their vibrationally excited states. Vibrational level populations in OCS molecules are approximately Boltzmann distributed. Formaldehyde demonstrates a very different, highly mode-specific vibrational population distribution, which is consistent with the fast vibrational energy redistribution facilitated by Coriolis interaction. Finally, acetaldehyde molecules are found to be vibrationally cold, likely due to the efficient relaxation enabled by the low-frequency internal rotor mode.

The CPmmW-deduced branching of pyrolysis reaction products can be compared with kinetics computer simulations to gain insight into the chemistry that occurs inside the reactor. Perhaps the most significant challenge in using the flash pyrolysis nozzle for dynamics and kinetics studies is the incomplete knowledge of the temperature and pressure distribution inside the reactor. In the present work we have attempted to elucidate some qualitative features of the flow in the reactor using the observed vibrational temperature distributions and simple kinetic estimates. Both experimental and theoretical the efforts to better characterize the reactor are under way in the groups of G. B. Ellison and J. W. Daily [91]. Photolysis-initiated unimolecular decomposition and more complex reactions would be another area of chemical reactivity addressed by the CP method. For unimolecular studies, a slit jet expansion provides a convenient environment, which provides sufficient rotational cooling of reaction products yet no secondary chemistry [48]. The pulsed uniform Laval flow, with well-characterized temperature and pressure [49], coupled with a CP spectrometer may prove to be the method of choice for studying complex chemical reactions that are important in atmosphere and in space. Finally, extension of the CPmmW spectrometer to cover the 100 – 200 GHz frequency region [31] in order to directly measure rotational temperature of smaller molecules is now both technologically possible and scientifically desirable.

References

1. M.C.L. Gerry, W. Lewisbevan, and N.P.C. Westwood, *The Microwave-Spectrum of an Unstable Molecule - Chloroketene ClHCCO.* Journal of Chemical Physics, 1983. **79**(10): p. 4655-4663.

2. P. Chen, S.D. Colson, W.A. Chupka, and J.A. Berson, *Flash Pyrolytic Production of Rotationally Cold Free-Radicals in a Supersonic Jet - Resonant Multiphoton Spectrum of the 3p2A" <-- X2A" Origin Band of CH3.* Journal of Physical Chemistry, 1986. **90**(11): p. 2319-2321.

3. J.R. Dunlop, J. Karolczak, and D.J. Clouthier, *Pyrolysis Jet Spectroscopy.* Chemical Physics Letters, 1988. **151**(4-5): p. 362-368.

4. J.I. Choe, S.R. Tanner, and M.D. Harmony, *Laser-Excitation Spectrum and Structure of CCl2 in a Free-Jet Expansion from a Heated Nozzle.* Journal of Molecular Spectroscopy, 1989. **138**(2): p. 319-331.

5. H.S. Gutowsky, J. Chen, P.J. Hajduk, J.D. Keen, and T. Emilsson, *The Silicon Carbon Double-Bond - Theory Takes a Round.* Journal of the American Chemical Society, 1991. **113**(13): p. 4747–4751.

6. D.W. Kohn, H. Clauberg, and P. Chen, *Flash Pyrolysis Nozzle for Generation of Radicals in a Supersonic Jet Expansion.* Review of Scientific Instruments, 1992. **63**(8): p. 4003-4005.

7. M.D. Harmony, K.A. Beren, D.M. Angst, and K.L. Ratzlaff, *Compact Hot-Nozzle Fourier-Transform Microwave Spectrometer.* Review of Scientific Instruments, 1995. **66**(11): p. 5196-5202.

8. M.R. Cameron and S.H. Kable, *A new design for a simple and effective pyrolysis nozzle in a supersonic free jet.* Review of Scientific Instruments, 1996. **67**(1): p. 283-287.

9. J. Kupper, J.M. Merritt, and R.E. Miller, *Free radicals in superfluid liquid helium nanodroplets: A pyrolysis source for the production of propargyl radical.* Journal of Chemical Physics, 2002. **117**(2): p. 647-652.

10. X. Zhang, A.V. Friderichsen, S. Nandi, G.B. Ellison, D.E. David, J.T. McKinnon, T.G. Lindeman, D.C. Dayton, and M.R. Nimlos, *Intense, hyperthermal source of organic radicals for matrix-isolation spectroscopy.* Review of Scientific Instruments, 2003. **74**(6): p. 3077-3086.

11.   Z.A. Liu, R.J. Livingstone, and P.B. Davies, *Pulse pyrolysis infrared laser jet spectroscopy of free radicals.* Chemical Physics Letters, 1998. **291**(5-6): p. 480-486.

12.   A. Vasiliou, M.R. Nimlos, J.W. Daily, and G.B. Ellison, *Thermal Decomposition of Furan Generates Propargyl Radicals.* Journal of Physical Chemistry A, 2009. **113**(30): p. 8540-8547.

13.   A.K. Vasiliou, K.M. Piech, B. Reed, X. Zhang, M.R. Nimlos, M. Ahmed, A. Golan, O. Kostko, D.L. Osborn, D.E. David, K.N. Urness, J.W. Daily, J.F. Stanton, and G.B. Ellison, *Thermal decomposition of CH3CHO studied by matrix infrared spectroscopy and photoionization mass spectroscopy.* Journal of Chemical Physics, 2012. **137**(16): p. 164308.

14.   A.K. Vasiliou, J.H. Kim, T.K. Ormond, K.M. Piech, K.N. Urness, A.M. Scheer, D.J. Robichaud, C. Mukarakate, M.R. Nimlos, J.W. Daily, Q. Guan, H.H. Carstensen, and G.B. Ellison, *Biomass pyrolysis: Thermal decomposition mechanisms of furfural and benzaldehyde.* Journal of Chemical Physics, 2013. **139**(10): p. 104310.

15.   K.N. Urness, Q. Guan, A. Golan, J.W. Daily, M.R. Nimlos, J.F. Stanton, M. Ahmed, and G.B. Ellison, *Pyrolysis of furan in a microreactor.* Journal of Chemical Physics, 2013. **139**(12): p. 124305.

16.   H.W. Rohrs, C.T. Wickhamjones, G.B. Ellison, D. Berry, and B.M. Argrow, *Fourier-Transform Infrared-Absorption Spectroscopy of Jet-Cooled Radicals.* Review of Scientific Instruments, 1995. **66**(3): p. 2430-2441.

17.   N. Savage, *The ideal biofuel.* Nature, 2011. **474**(7352): p. S9-S11.

18.   M.K. Bahng, C. Mukarakate, D.J. Robichaud, and M.R. Nimlos, *Current technologies for analysis of biomass thermochemical processing: A review.* Analytica Chimica Acta, 2009. **651**(2): p. 117-138.

19.   M. Inman, *News Feature: Cooking up Fuel.* Nature Climate Change, 2012. **2**(4): p. 218-220.

20.   T.A. Cool, K. Nakajima, T.A. Mostefaoui, F. Qi, A. McIlroy, P.R. Westmoreland, M.E. Law, L. Poisson, D.S. Peterka, and M. Ahmed, *Selective detection of isomers with photoionization mass spectrometry for studies of hydrocarbon flame chemistry.* Journal of Chemical Physics, 2003. **119**(16): p. 8356-8365.

21.   A.J. Trevitt, M.B. Prendergast, F. Goulay, J.D. Savee, D.L. Osborn, C.A. Taatjes, and S.R. Leone, *Product Branching Fractions of the CH plus Propene Reaction from Synchrotron Photoionization Mass Spectrometry.* Journal of Physical Chemistry A, 2013. **117**(30): p. 6450-6457.

22.   J.F. Lockyear, O. Welz, J.D. Savee, F. Goulay, A.J. Trevitt, C.A. Taatjes, D.L. Osborn, and S.R. Leone, *Isomer Specific Product Detection in the Reaction of CH with Acrolein.* Journal of Physical Chemistry A, 2013. **117**(43): p. 11013-11026.

23. P.A. Heimann, M. Koike, C.W. Hsu, D. Blank, X.M. Yang, A.G. Suits, Y.T. Lee, M. Evans, C.Y. Ng, C. Flaim, and H.A. Padmore, *Performance of the vacuum ultraviolet high-resolution and high-flux beamline for chemical dynamics studies at the Advanced Light Source.* Review of Scientific Instruments, 1997. **68**(5): p. 1945-1951.

24. D.L. Osborn, P. Zou, H. Johnsen, C.C. Hayden, C.A. Taatjes, V.D. Knyazev, S.W. North, D.S. Peterka, M. Ahmed, and S.R. Leone, *The multiplexed chemical kinetic photoionization mass spectrometer: A new approach to isomer-resolved chemical kinetics.* Review of Scientific Instruments, 2008. **79**(10): p. 104103.

25. J. Wang, B. Yang, T.A. Cool, N. Hansen, and T. Kasper, *Near-threshold absolute photoionization cross-sections of some reaction intermediates in combustion.* International Journal of Mass Spectrometry, 2008. **269**(3): p. 210-220.

26. B. Yang, J. Wang, T.A. Cool, N. Hansen, S. Skeen, and D.L. Osborn, *Absolute photoionization cross-sections of some combustion intermediates.* International Journal of Mass Spectrometry, 2012. **309**: p. 118-128.

27. L. Yan, F. Curdy, W. Li, and A.G. Suits, *Isomer-Specific Mass Spectrometric Detection Via "Semisoft" Strong-Field Ionization.* Journal of physical chemistry A, 2013. **117**: p. 11890−11895.

28. G.G. Brown, B.C. Dian, K.O. Douglass, S.M. Geyer, S.T. Shipman, and B.H. Pate, *A broadband Fourier transform microwave spectrometer based on chirped pulse excitation.* Review of Scientific Instruments, 2008. **79**(5): p. 053103.

29. D.P. Zaleski, J.L. Neill, M.T. Muckle, N.A. Seifert, P.B. Carroll, S.L.W. Weaver, and B.H. Pate, *A K-a-band chirped-pulse Fourier transform microwave spectrometer.* Journal of Molecular Spectroscopy, 2012. **280**: p. 68-76.

30. B.C. Dian, G.G. Brown, K.O. Douglass, F.S. Rees, J.E. Johns, P. Nair, R.D. Suenram, and B.H. Pate, *Conformational isomerization kinetics of pent-1-en-4-yne with 3,330 cm(-1) of internal energy measured by dynamic rotational spectroscopy.* Proceedings of the National Academy of Sciences of the United States of America, 2008. **105**(35): p. 12696-12700.

31. A.L. Steber, B.J. Harris, J.L. Neill, and B.H. Pate, *An arbitrary waveform generator based chirped pulse Fourier transform spectrometer operating from 260 to 295 GHz.* Journal of Molecular Spectroscopy, 2012. **280**: p. 3-10.

32. J.L. Neill, K.O. Douglass, B.H. Pate, and D.W. Pratt, *Next generation techniques in the high resolution spectroscopy of biologically relevant molecules.* Physical Chemistry Chemical Physics, 2011. **13**(16): p. 7253-7262.

33. J.L. Neill, B.J. Harris, A.L. Steber, K.O. Douglass, D.F. Plusquellic, and B.H. Pate, *Segmented chirped-pulse Fourier transform submillimeter spectroscopy for broadband gas analysis.* Optics Express, 2013. **21**(17): p. 19743-19749.

34. B.H. Pate and F.C. De Lucia, *Broadband Molecular Rotational Spectroscopy Special Issue Introduction.* Journal of Molecular Spectroscopy, 2012. **280**: p. 1-2.

35.   G.B. Park, A.H. Steeves, K. Kuyanov-Prozument, J.L. Neill, and R.W. Field, *Design and evaluation of a pulsed-jet chirped-pulse millimeter-wave spectrometer for the 70-102 GHz region.* Journal of Chemical Physics, 2011. **135**(2): p. 024202.

36.   C.H. Townes and A.L. Schawlow, *Microwave Spectroscopy.* 1955, New York: McGraw-Hill Book Company.

37.   D. Patterson, M. Schnell, and J.M. Doyle, *Enantiomer-specific detection of chiral molecules via microwave spectroscopy.* Nature, 2013. **497**(7450): p. 475.

38.   B.C. Dian, G.G. Brown, K.O. Douglass, and B.H. Pate, *Measuring picosecond isomerization kinetics via broadband microwave spectroscopy.* Science, 2008. **320**(5878): p. 924-928.

39.   T.J. Balle and W.H. Flygare, *Fabry-Perot Cavity Pulsed Fourier-Transform Microwave Spectrometer with a Pulsed Nozzle Particle Source.* Review of Scientific Instruments, 1981. **52**(1): p. 33-45.

40.   R.D. Suenram, J.U. Grabow, A. Zuban, and I. Leonov, *A portable, pulsed-molecular-beam, Fourier-transform microwave spectrometer designed for chemical analysis.* Review of Scientific Instruments, 1999. **70**(4): p. 2127-2135.

41.   J.C. Mcgurk, T.G. Schmalz, and W.H. Flygare, *Fast Passage in Rotational Spectroscopy - Theory and Experiment.* Journal of Chemical Physics, 1974. **60**(11): p. 4181-4188.

42.   J.C. Mcgurk, R.T. Hofmann, and W.H. Flygare, *Transient Absorption and Emission and Measurement of T1 and T2 in J0-]1 Rotational Transition in OCS.* Journal of Chemical Physics, 1974. **60**(7): p. 2922-2928.

43.   R.L. Shoemaker, in *Laser and Coherence Spectroscopy*, J.I. Steinfeld, Editor. 1978, Plenum Press: New York.

44.   D. Schmitz, V.A. Shubert, T. Betz, and M. Schnell, *Multi-resonance effects within a single chirp in broadband rotational spectroscopy: The rapid adiabatic passage regime for benzonitrile.* Journal of Molecular Spectroscopy, 2012. **280**: p. 77-84.

45.   V.M. Akulin and N.V. Karlov, *Intense Resonant Interactions in Quantum Electronics.* 1992, Berlin: Springer-Verlag.

46.   M. Schnell, *Broadband Rotational Spectroscopy for Molecular Structure and Dynamics Studies.* Zeitschrift Fur Physikalische Chemie-International Journal of Research in Physical Chemistry & Chemical Physics, 2013. **227**(1): p. 1-21.

47.   B.H. Pate and F.C. De Lucia, *Special issue of journal of molecular spectroscopy focusing on developments in broadband rotational spectroscopy.* Journal of Molecular Spectroscopy, 2011. **269**(1): p. 1-1.

48. K. Prozument, R.G. Shaver, M.A. Ciuba, J.S. Muenter, G.B. Park, J.F. Stanton, H. Guo, B.M. Wong, D.S. Perry, and R.W. Field, *A New Approach toward Transition State Spectroscopy.* Faraday Discussions, 2013. **163**: p. 33-57.

49. I.R. Sims, J.L. Queffelec, A. Defrance, C. Rebrionrowe, D. Travers, P. Bocherel, B.R. Rowe, and I.W.M. Smith, *Ultralow Temperature Kinetics of Neutral-Neutral Reactions - the Technique and Results for the Reactions Cn+O-2 down to 13 K and Cn+Nh3 down to 25 K.* Journal of Chemical Physics, 1994. **100**(6): p. 4229-4241.

50. H. Lee, J.H. Baraban, R.W. Field, and J.F. Stanton, *High-Accuracy Estimates for the Vinylidene-Acetylene Isomerization Energy and the Ground State Rotational Constants of :C=CH2.* Journal of Physical Chemistry A, 2013. **117**: p. 11679–11683.

51. K. Prozument, A.P. Colombo, Y. Zhou, G.B. Park, V.S. Petrovic, S.L. Coy, and R.W. Field, *Chirped-Pulse Millimeter-Wave Spectroscopy of Rydberg-Rydberg Transitions.* Physical Review Letters, 2011. **107**(14): p. 143001.

52. A.P. Colombo, Y. Zhou, K. Prozument, S.L. Coy, and R.W. Field, *Chirped-pulse millimeter-wave spectroscopy: Spectrum, dynamics, and manipulation of Rydberg-Rydberg transitions.* Journal of Chemical Physics, 2013. **138**(1).

53. J.B. Levy, *The Thermal Decomposition of Ethyl Nitrite.* Journal of the American Chemical Society, 1956. **78**(9): p. 1780-1783.

54. L. Batt and R.T. Milne, *Gas-Phase Pyrolysis of Alkyl Nitrites .4. Ethyl Nitrite.* International Journal of Chemical Kinetics, 1977. **9**(4): p. 549-565.

55. P.H. Turner, M.J. Corkill, and A.P. Cox, *Microwave-Spectra and Structures of Cis-Methyl Nitrite and Trans-Methyl Nitrite - Methyl Barrier in Trans-Methyl Nitrite.* Journal of Physical Chemistry, 1979. **83**(11): p. 1473-1482.

56. C.M. Western, *PGOPHER, a Program for Simulating Rotational Structure*, 2010, University of Bristol: http://pgopher.chm.bris.ac.uk.

57. L. Batt, K. Christie, R.T. Milne, and A.J. Summers, *Heats of Formation of C1-C4 Alkyl Nitrites (Rono) and Their Ro-No Bond-Dissociation Energies.* International Journal of Chemical Kinetics, 1974. **6**(6): p. 877-885.

58. L. Batt, *Gas-Phase Decomposition of Alkoxy Radicals.* International Journal of Chemical Kinetics, 1979. **11**(9): p. 977-993.

59. H.J. Curran, *Rate constant estimation for C-1 to C-4 alkyl and alkoxyl radical decomposition.* International Journal of Chemical Kinetics, 2006. **38**(4): p. 250-275.

60. I. Kleiner, F.J. Lovas, and M. Godefroid, *Microwave spectra of molecules of astrophysical interest .23. Acetaldehyde.* Journal of Physical and Chemical Reference Data, 1996. **25**(4): p. 1113-1210.

61. H.M. Pickett, R.L. Poynter, E.A. Cohen, M.L. Delitsky, J.C. Pearson, and H.S.P. Muller, *Submillimeter, millimeter, and microwave spectral line catalog.* Journal of Quantitative Spectroscopy & Radiative Transfer, 1998. **60**(5): p. 883-890.

62. S. Saito and K. Takagi, *Microwave-Spectrum of Nitroxyl.* Journal of Molecular Spectroscopy, 1973. **47**(1): p. 99-106.

63. C.B. Moore, *A spectroscopist's view of energy states, energy transfers, and chemical reactions.* Annual Review of Physical Chemistry, 2007. **58**: p. 1-33.

64. G.M. Mcclelland, K.L. Saenger, J.J. Valentini, and D.R. Herschbach, *Vibrational and Rotational Relaxation of Iodine in Seeded Supersonic Beams.* Journal of Physical Chemistry, 1979. **83**(8): p. 947-959.

65. R.P. Mariella, S.K. Neoh, D.R. Herschbach, and W. Klemperer, *Vibrational-Relaxation in Seeded Supersonic Alkali-Halide Beams.* Journal of Chemical Physics, 1977. **67**(7): p. 2981-2985.

66. R.L. Deleon and J.S. Muenter, *Vibrational-Relaxation of Linear-Molecules in a Nozzle Expansion.* Chemical Physics Letters, 1984. **111**(1-2): p. 147-150.

67. N.J.G. Smith, C.C. Davis, and I.W.M. Smith, *Studies of Vibrational-Relaxation in Ocs and Cf4 by Pulsed Photoacoustic Techniques.* Journal of Chemical Physics, 1984. **80**(12): p. 6122-6133.

68. K. Tanaka, H. Ito, and T. Tanaka, *Millimeter Wave Spectroscopy of Ocs in Vibrationally Excited-States.* Journal of Molecular Spectroscopy, 1984. **107**(2): p. 324-332.

69. A. Fayt, R. Vandenhaute, and J.G. Lahaye, *Global Rovibrational Analysis of Carbonyl Sulfide.* Journal of Molecular Spectroscopy, 1986. **119**(2): p. 233-266.

70. I. Shamah and G. Flynn, *Translational and Vibrational Energy-Distributions in Metastable Laser Pumped Polyatomic-Molecules - Quasi-Thermodynamic Description.* Journal of Chemical Physics, 1978. **69**(6): p. 2474-2491.

71. G.W. Flynn, *Collision-Induced Energy-Flow between Vibrational-Modes of Small Polyatomic-Molecules.* Accounts of Chemical Research, 1981. **14**(11): p. 334-341.

72. B.M. Hopkins, Baronavs.A, and H.L. Chen, *Vibrational Relaxation of Ocs in Hbr, Hcl, and Rare Gaseous Mixtures.* Journal of Chemical Physics, 1973. **59**(2): p. 836-841.

73. M.L. Mandich and G.W. Flynn, *Collisional Relaxation of Vibrationally Excited Ocs in Rare-Gas Mixtures.* Journal of Chemical Physics, 1980. **73**(8): p. 3679-3687.

74. M.L. Mandich and G.W. Flynn, *Vibrational Energy-Transfer Map for Ocs.* Journal of Chemical Physics, 1980. **73**(3): p. 1265-1279.

75. R.J. Bouwens, J.A. Hammerschmidt, M.M. Grzeskowiak, T.A. Stegink, P.M. Yorba, and W.F. Polik, *Pure vibrational spectroscopy of S-0 formaldehyde by dispersed fluorescence.* Journal of Chemical Physics, 1996. **104**(2): p. 460-479.

76. R. Bocquet, J. Demaison, L. Poteau, M. Liedtke, S. Belov, K.M.T. Yamada, G. Winnewisser, C. Gerke, J. Gripp, and T. Kohler, *The ground state rotational spectrum of formaldehyde.* Journal of Molecular Spectroscopy, 1996. **177**(1): p. 154-159.

77. T. Oka, Y. Morino, and K. Takagi, *Microwave Spectrum of Formaldehyde in Vibrationally Excited States.* Journal of Molecular Spectroscopy, 1964. **14**(1): p. 27.

78. F. Ito, T. Nakanaga, and H. Takeo, *Ftir Spectra of the 2-Nu(4), Nu(4)+Nu(6) and 2-Nu(6) Bands of Formaldehyde.* Spectrochimica Acta Part a-Molecular and Biomolecular Spectroscopy, 1994. **50**(8-9): p. 1397-1412.

79. H.L. Dai, C.L. Korpa, J.L. Kinsey, and R.W. Field, *Rotation-Induced Vibrational Mixing in X1a1 Formaldehyde - Non-Negligible Dynamical Consequences of Rotation.* Journal of Chemical Physics, 1985. **82**(4): p. 1688-1701.

80. D.M. Smith, *Vibration-rotation interactions between overtone and combination levels of asymmetric-top molecules: Application to the infrared spectroscopy of formaldehyde and ketene.* Journal of Chemical Physics, 2005. **122**(3): p. 034307.

81. W.O. George, B.F. Jones, R. Lewis, and J.M. Price, *Ab initio computations on simple carbonyl compounds.* Journal of Molecular Structure, 2000. **550**: p. 281-296.

82. K.B. Wiberg, Y. Thiel, L. Goodman, and J. Leszczynski, *Acetaldehyde - Harmonic Frequencies, Force-Field, and Infrared Intensities.* Journal of Physical Chemistry, 1995. **99**(38): p. 13850-13864.

83. F.C. Delucia and P.A. Helminger, *Millimeter-Wave Spectroscopy of Active Laser Plasmas - Excited Vibrational-States of Hcn.* Journal of Chemical Physics, 1977. **67**(9): p. 4262-4267.

84. K. Raghavachari, G.W. Trucks, J.A. Pople, and M. Headgordon, *A 5th-Order Perturbation Comparison of Electron Correlation Theories.* Chemical Physics Letters, 1989. **157**(6): p. 479-483.

85. L. McCaslin and J.F. Stanton, Molecular Physics, 2013(submitted).

86. J. Almlof and P.R. Taylor, *General Contraction of Gaussian-Basis Sets .1. Atomic Natural Orbitals for 1st-Row and 2nd-Row Atoms.* Journal of Chemical Physics, 1987. **86**(7): p. 4070-4077.

87. C. Puzzarini, J.F. Stanton, and J. Gauss, *Quantum-chemical calculation of spectroscopic parameters for rotational spectroscopy.* International Reviews in Physical Chemistry, 2010. **29**(2): p. 273-367.

88.   G.A. Bethardy, X.L. Wang, and D.S. Perry, *The Role of Molecular Flexibility in Accelerating Intramolecular Vibrational-Relaxation.* Canadian Journal of Chemistry-Revue Canadienne De Chimie, 1994. **72**(3): p. 652-659.

89.   J.B. Pedley, R.D. Naylor, and S.P. Kirby, *Thermochemical Data of Organic Compounds*, ed. n. ed. 1986, London, New York: Chapman and Hall.

90.   J. Kestin, K. Knierim, E.A. Mason, B. Najafi, S.T. Ro, and M. Waldman, *Equilibrium and Transport-Properties of the Noble-Gases and Their Mixtures at Low-Density.* Journal of Physical and Chemical Reference Data, 1984. **13**(1): p. 229-303.

91.   Q. Guan, G.B. Ellison, and J.W. Daily, in preparation, 2014.